Geophys. J. Int. (2009) **178,** 180–194 doi: 10.1111/j.1365-246X.2008.04058.x

The tsunami of 2007 September 12, Bengkulu province, Sumatra, Indonesia: post-tsunami field survey and numerical modelling

Jose C. Borrero,[1,2] Robert Weiss,[3] Emile A. Okal,[4] Rahman Hidayat,[5,6] Suranto,[5] Diego Arcas[7,8] and Vasily V. Titov[7,8]

[1]*ASR Ltd., Marine Consulting and Research, Raglan, New Zealand. E-mail: jborrero@usc.edu*
[2]*Tsunami Research Center, University of Southern California, Los Angeles, CA, USA*
[3]*Department of Geology and Geophysics, Texas A&M University, College Station,* TX 77843*, USA*
[4]*Department of Earth and Planetary Sciences, Northwestern University, Evanston,* IL 60208*, USA*
[5]*Coastal Engineering Laboratory-BPPT, J1. Grafika* 2*, Yogyakarta* 55281*, Indonesia*
[6]*Presently at: Meguro Laboratory, Institute of Industrial Science—The University of Tokyo, Komaba* 4-6-1*, Meguro-ku, Tokyo* 153-8505*, Japan and Institute for Sustainability and Peace-United Nations University (UNU-ISP), Shibuya-ku, Tokyo* 150-8925*, Japan*
[7]*NOAA Center for Tsunami Research,* 7600 *Sand Point Way, Seattle,* WA 98195*, USA*
[8]*Joint Institute for the Study of the Atmosphere and Ocean, University of Washington, Seattle,* WA 98195*, USA*

Accepted 2008 December 2. Received 2008 November 9; in original form 2008 June 16

SUMMARY

The $M_w = 8.4$ earthquake on 2007 September 12, offshore of the Bengkulu province of Sumatra, Indonesia, generated a moderate tsunami with run-up heights of up to 4 m as measured by Indonesian and international researchers in the days following the earthquake. The tsunami was observed along 250 km of coastline and caused damage at several locations. The largest wave heights and most severe inundation were observed about 50 km to the northwest of Bengkulu; elsewhere the effects were less severe—with the exception of substantial inundation at a site 150 km to the south. In addition to presenting the field data, we conduct a modelling study and compare the run-up heights and water-level predictions from four different seismic deformation models used to initialize a tsunami propagation and inundation model. Our comparative results suggest that, for this event, the estimates of fault parameters available immediately after determination of the earthquake size and location predicted the near-field run-up heights and distribution and far-field wave equally well as estimates obtained using more detailed descriptions of the seafloor deformation, as typically available hours or days after an event. We conclude that while detailed slip patterns can be important to the near-field run-up distribution, simple fault models can be used to rapidly assess the likely near- and far-field tsunami effects of a particular earthquake.

Key words: Tsunamis; Earthquake source observations; Seismicity and tectonics; Early warning; Subduction zone processes; Submarine tectonics.

1 INTRODUCTION

The Sumatra subduction zone (SSZ) (Fig. 1) and its prolongation northward along the Nicobar–Andaman arc are host to powerful earthquakes generating destructive tsunamis as documented by recent events, historical accounts and palaeoseismic evidence (Zachariasen *et al.* 1999; Borrero, 2005; Natawidjaja *et al.* 2007), although the information remains scant regarding the possible recurrence rate of the largest events. In this framework, a series of significant earthquakes took place on 2007 September 12–13 (Fig. 2). Event I (the first and largest; 4.52°S and 101.37°E; $M_w = 8.4$) took place at 18:10 local time (11:10 UTC) on the 12th, offshore of Bengkulu province Sumatra; a large aftershock (Event II; 2.7°S and 100.7° E; $M_w = 7.9$) followed at 23:49 UTC, and a third shock (Event III; 2.3°S and 99.6°E; $M_w = 7.1$) took place at 03:35 UTC on the 13th (10:35 local time). Strictly speaking, the latter should not be called an aftershock, since most tomographic source models (e.g., Ji (2007)) place it outside the area of rupture of the main shock.

The SSZ has been the site of three catastrophic tsunamigenic earthquakes in the past 175 years. The Sumatra–Andaman earthquake of 2004 December 26 was the second or third largest seismic event ever recorded (Nettles *et al.* 2005; Stein & Okal 2005) and its tsunami probably the most lethal one in the history of mankind. The Nias–Simeulue earthquake of 2005 March 28 ($M_w = 8.7$) is best remembered on two accounts; first its successful anticipation based on the concept of Coulomb stress transferred from the 2004 rupture zone (McCloskey *et al.* 2005), and second its lack of a significant tsunami in the far field, despite its very large seismic moment (the earthquake would have been the largest one in 40 years, but for the 2004 shock), which prompted wild speculation and nervous evacuation throughout the Indian Ocean Basin.

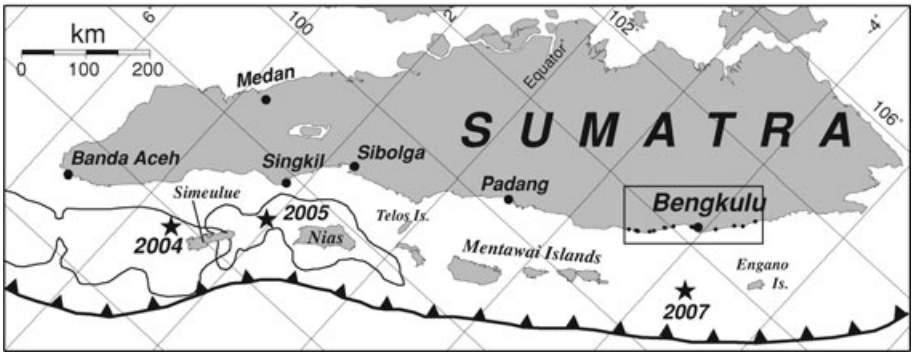

Figure 1. A location map of Sumatra. The stars indicate the epicentres of the 2004, 2005 and 2007 earthquakes. The thin irregular black lines represent the ruptures of the December 2004 and March 2005 earthquakes, slip was >1 m inside the lines. The barbed line is the seafloor trace of the Sunda megathrust, which dips beneath Sumatra. The 2006 tsunami primarily affected the coast near Bengkulu; the field survey locations are indicated by the black dots inside the box near Bengkulu.

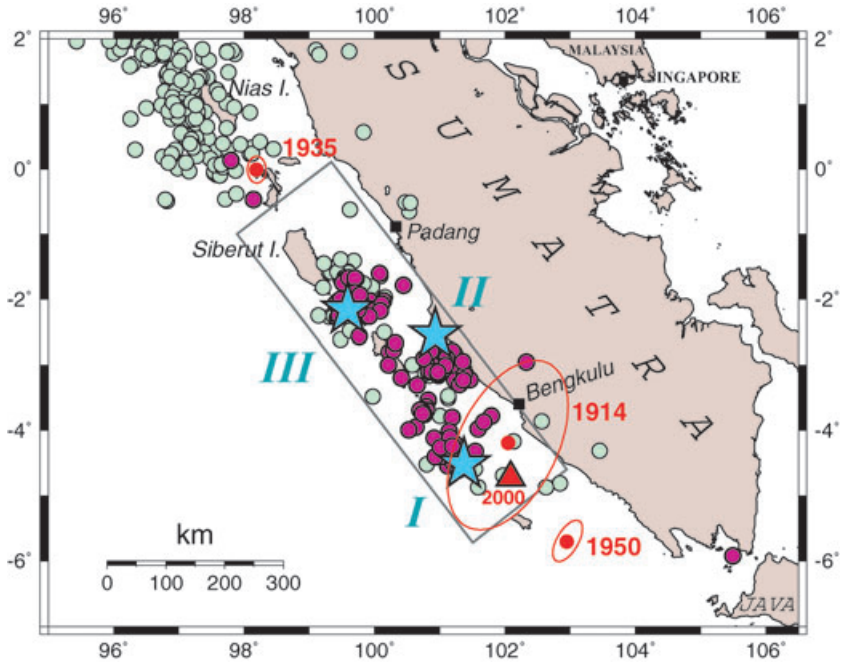

Figure 2. Map of the epicentral area of the 2007 Bengkulu series. The grey rectangle is the fault zone of the 1833 event, as inferred by Zachariasen *et al.* (1999). The three large stars are the epicentres of the 2007 September 12 main shock (11:10 UTC; I), of its main after shock at 23:49 UTC (II) and of the third large event at 03:35 on September 13 (III). The purple dots show the PDE locations of their aftershocks up to 2007 September 29. Global CMT solutions posterior to the 2004 Sumatra–Andaman earthquake are shown as light green dots. Relocated historical earthquakes are shown as solid red dots with associated Monte Carlo ellipses. The triangle identifies the 2000 earthquake.

Nevertheless, a damaging local tsunami was generated, which affected Nias, Simeulue and the Banyak Islands, as well as Singkil on the Sumatran coast (Borrero, unpublished field notes), fortunately resulting in very little loss of life, thanks to an orderly evacuation by coastal populations (McAdoo *et al.* 2006). Subsequent numerical modelling showed that the far-field amplitude of this tsunami remained at benign levels, since it was muted by the large fraction of coseismic displacement that occurred either directly under Nias Island and thus not contributing to tsunami generation or in very shallow bathymetry resulting in tsunami amplitudes faltering at the transition to the deep waters of the Indian Ocean Basin (Geist *et al.* 2006; Okal & Synolakis 2008).

The third catastrophic event documented historically in the area is the Sumatra earthquake of 1833 November 24, for which there are of course no seismic records, but whose source mechanism was reconstructed by Zachariasen *et al.* (1999) on the basis of the mapping of uplifted corals on the Mentawai Islands offshore of Sumatra. The resulting seismic moment (7×10^{29} dyn-cm) and seismic slip (13 m) make it a truly gigantic shock, supporting the reports of a locally devastating tsunami from Pariaman to Bengkulu (Wichmann 1918). In the far field, the 1833 tsunami inflicted damage in the Seychelles on a level comparable to that in 2004 (Jackson *et al.* 2005), which suggests that it was similarly destructive over the entire Indian Ocean Basin, where historical records are mostly non-existent for this period.

In the aftermath of the 2005 Nias earthquake, Nalbant *et al.* (2005) again used the concept of Coulomb stress transfer to suggest enhanced stress in the epicentral area of the 1833 earthquake, which

according to plate kinematic models (Chamot-Rooke & Le Pichon 1999; Socquet *et al.* 2006) had accumulated 9 m of convergence since 1833. Accordingly, the area was considered ripe for a major event (Pollitz 2006), possibly as large as a repeat of the 1833 shock. The 1833 model was widely used as a worst-case, but realistic and historically proven, scenario for the numerical simulation of the near- and far-field effects of tsunamis generated from potential future earthquakes in the area (Borrero *et al.* 2006; McCloskey *et al.* 2008; Okal & Synolakis 2008).

In this framework, the initial location of Event I was of particular concern, as it occurred on a section of subduction zone located between the Mentawai and Engano Islands (Fig. 1), and thus deprived of the topographic features that had lessened the impact of the 2005 Nias tsunami in the far field (Borrero *et al.* 2006). Thus, the warning centres worked feverishly and the world waited anxiously in the hours after Event I to assess its tsunami and, in particular, its potential in the far field. Only two maregraphic stations, Padang and Sibolga (See Fig. 1) reported tsunami amplitudes from the immediate source region. The first confirmation of a tsunami, with an amplitude of 0.35 m at Padang, came 70 min after origin time and was later revised to 0.56 m at 13:06 UTC, and then again to 0.90 m at 13:48. Final reports from the Pacific Tsunami Warning Center gave a peak-to-trough total wave height of 2.27 m at Padang. While the amplitude at Sibolga was small (0.09 m at 14:34 UTC), the metric amplitude at Padang was itself of concern, as the station lay along strike from the earthquake source, a notoriously unfavourable geometry. In the regional field, the Cocos Island tidal station (12.1°S and 96.9°E; 938 km from the epicentre) reported a tsunami amplitude of 0.11 m at 12:36 UTC, alleviating somewhat the fears of a devastating basinwide tsunami. This was further reinforced at 14:21 UTC when the Deep Ocean Recording of Tsunami (DART) 23401 buoy reported a mere 0.02-m amplitude; however, its location (8.9°N; 88.5°E) was again at an unfavourable azimuth from the source.

In the meantime, one of the authors (EAO) carried out a customized, unofficial assessment of the earthquake's long-period characteristics using a number of real-time methods (Weinstein & Okal 2005), which led to a preliminary moment of 5×10^{28} dyn-cm, that was then used to model in real time the effect of the tsunami on the western coasts of the Indian Ocean. In particular, the resulting value of less than 2 cm for the tsunami amplitude in deep water off the coast of South Africa was transmitted to a local colleague and used to call off what amounted to a tsunami watch in that country (Hartnady & Okal 2007). This moment value, later confirmed by the QUICK solution of the Global Centroid Moment Tensor project ($M_0 = 5.05 \times 10$ sup^{28} dyn-cm), clearly indicates that the 2007 Bengkulu earthquake was not the anticipated repeat of the 1833 event. As discussed, for example, in the appendix of Okal & Synolakis (2008), the 2007 fault rupture zone extends over no more than 200 km and thus fails to cover the full extent of the 1833 fault. This result, readily apparent from the distribution of the aftershocks immediately following Event I (and not including the more distant Event III), is supported by detailed source tomography investigations (Ji 2007). In addition, the latter have shown that the seismic slip (on the average 5 m) also falls short of the estimated 9 m accumulated since 1833. In summary, with respect to the 1833 scenario, the 2007 rupture is deficient both in fault extent (it leaves large segments untouched) and in slip (it does not even fully clean up its actual rupture area).

This has two consequences: it explains the somewhat moderate near-field tsunami and the benign one in the far field; and it suggests that substantial portions of the 1833 rupture still bear significant accumulations of strain which could be released in a future large earthquake. In this respect, the partially released source area of the 2007 Bengkulu does not necessarily constitute a barrier to a future rupture, as documented, for example, by the case of the 2004 Sumatra–Andaman mega-event, whose fault extended over and beyond (in lay terms, 'jumped') the rupture area of the Car-Nicobar earthquake of 1881 and of the smaller Andaman earthquake of 1941 (Ortiz & Bilham 2003). In other words, the 2007 Bengkulu may have somewhat altered the potential for a mega-earthquake in the region, but it certainly has not eliminated it (Okal & Synolakis 2008).

In the days following the Bengkulu events, there were no media reports of widespread tsunami destruction, neither in the near nor in the far field. While the Bengkulu shoreline was spared the catastrophic level of destruction envisioned under a worst-case scenario, it was evident that a tsunami of locally relevant amplitude had been generated, and thus a field survey was organized along the now classical practices reviewed, for example, by Synolakis & Okal (2005).

2 POST-TSUNAMI FIELD SURVEY

The survey commenced on the morning of September 15, less than 3 d after the earthquake and covered approximately 300 km of the Sumatra coast centred on the city of Bengkulu. The survey team was comprised of two local and one foreign tsunami scientist, all with extensive prior experience in post-tsunami field surveys. The team measured flow depths and tsunami heights, maximum run-up, inundation distances, recorded structural damage and interviewed eyewitnesses as per established methods (Synolakis & Okal 2005). The measured data were corrected to the tide level at the time of the earthquake. Inspection of tidal data showed that the earthquake occurred near high tide; thus, a negative correction to field run-up measurements was performed, its amplitude varying up to 0.8 m depending on the exact survey time of each datum. Fortunately, the tsunami was not large, as the tidal level would have made the inundation far worse.

The measured tsunami run-up data are summarized in Fig. 3 and listed in Table 1. In general, the measured tsunami heights were typically around 2 m and did not exceed 4 m. The area most strongly affected was to the north of Bengkulu between Lais and Karang Pulau. The tsunami heights were below the threshold of the beach berm at the northern and southern extents of our observations. It is possible that tsunami heights could be even larger to the north of Ipuh; however, this area could not be accessed due to time constraints. Another survey group reported a tsunami run-up height of 3.6 m at MukoMuko, located north of Ipuh (BMG Team, personal communication). However, it had not been confirmed whether this value has been corrected for the tide level.

2.1 Bengkulu and vicinity

Five locations were surveyed in the vicinity of Bengkulu, including sites in the city itself as well as around Pulau Baai Harbor to the south. The coastline in the immediate vicinity of Bengkulu is characterized by a series of headlands that are similar in shape and proportions, and diminish in size from south to north (Fig. 4). The city of Bengkulu occupies the central headland, while the southern headland features a large lagoon containing two commercial and one fishing port. Near Bengkulu, tsunami measurements were collected at four locations—on the exposed southwest-facing coast,

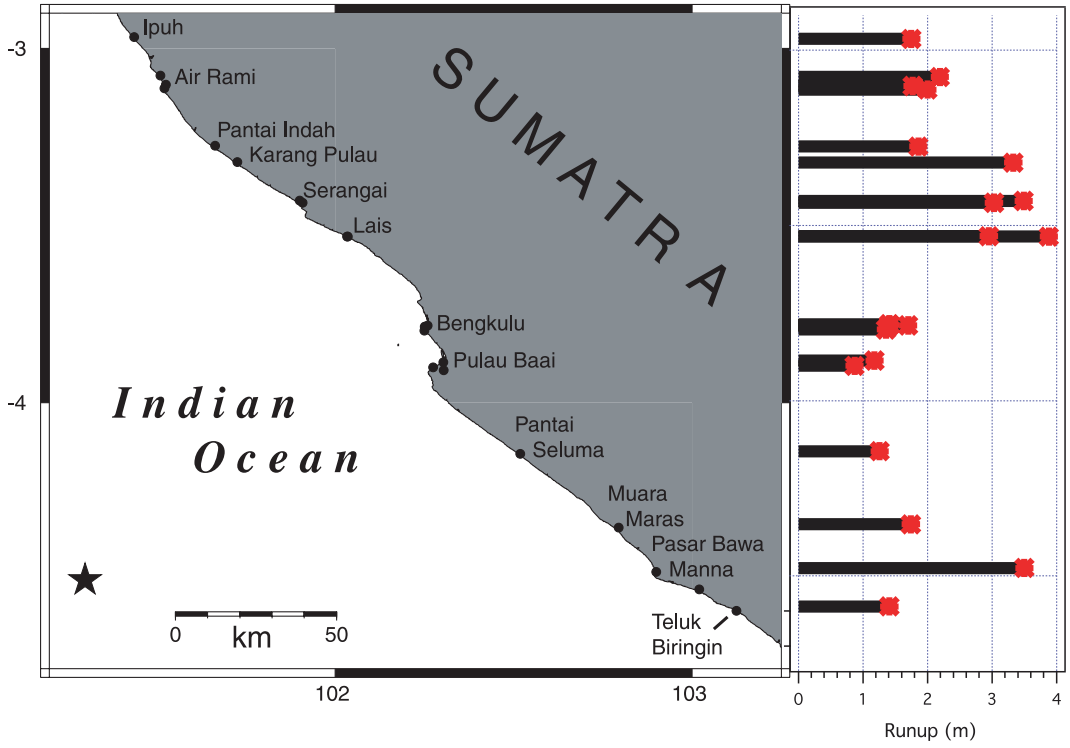

Figure 3. Summary of run-up values measured along the coast of southwestern Sumatra. Detailed time series from the models were extracted from locations offshore of Air Rami, Serangai, Bengkulu and Muara Maras.

two locations in the fishing port at the extreme western tip of the headland and in a small village in the sheltered cove.

At the exposed beach 'Pantai Nala', local residents reported that the largest positive surges came between 8 and 10 p.m. but did not rise above the level of a concrete seawall that had been installed along the beachfront. A small fishing boat that was pushed against the seawall had been there since before the event and was not moved as a result of the tsunami. Residents indicated that during large swells and storms, the water level reaches the seawall. Therefore, we conjectured that the maximum run-up at Pantai Nala is constrained to be no more than 2.0 m.

At the small Bengkulu port (Tapak Paderi), local fishermen indicated the maximum tsunami water levels. Most interviewees reported that they did not observe the inundation directly because they had evacuated after the earthquake, returning afterwards to check the condition of their boats. A fisherman reported that the surge rose to a level indicated on the staircase leading down to the docks. The dock level was overtopped and there was some flooding, indicated by flow marks and debris, but no damage reported to the dock structures. One witness who did observe the tsunami, reported waves at 8:30, 9:00 and 9:30 p.m., with the largest wave arriving last. At the next location, also part of the port complex, witnesses provided a clearer description of the event, reporting that the sea began to recede shortly after the earthquake, taking at least 15 min to go out, returning 30 min later. This witness reported a total of five surges, but could not indicate which was the largest.

Further north, at Pantai Jakat, the tsunami run-up was measured in a small settlement located in the protected lee of the Bengkulu headland. Here, the residents had a very clear observation of the tsunami effects. They reported that the first wave arrived some 15 min after the earthquake, and then withdrew before returning to a level higher than the first surge approximately 1 hr after the first wave. This surge then retreated, and 1 hr later the third and largest surge arrived. This would put the arrival of the largest wave approximately 2.5 hr after the earthquake or approximately 8:30 p.m. local time (13:30 UTC).

To the south of Bengkulu is Pulau Baai Harbor. The harbour was created in the early 1980s when a channel was cut through the northern barrier beach, connecting the lagoon to the sea. There are two commercial ports located in the harbour and a large fishing port. At the port administrative offices, there was evidence of strong ground shaking and significant structural damage. Large shear cracks were observed in the walls of the warehouse as well as significant settlement cracks in the administrative building itself. On the grounds of the complex, there was evidence of liquefaction through cracks in the ground as well as sand boils that measured several meters in diameter.

Discussions with crewmembers from a civilian tugboat as well as from a military patrol boat were similar in that neither crew reported significant water level changes, overtopping of the wharf or boats touching bottom. The tugboat crew reported some change in the water level, saying the water withdrew first shortly after the earthquake (5 min) and then returned slowly some 2 hr later. He did indicate that the boat was sitting higher in the water relative to the dock than before the earthquake, suggesting local subsidence. The captain of the military patrol boat was less descriptive and insisted that there was very little if any changes to the water level after the earthquake and that the boat's position relative to the dock had not changed. His claim was supported by our inspection of the pier piles, which showed the current water level to be compatible with water levels indicated by marine growth on the piles.

Two locations were surveyed along the open coast to the west of the harbour. On the sandy beach south of the harbour entrance jetty, a clear debris line was observed beyond the low beach berm.

Table 1. Measured run-up.

Date/time	Longitude (°E)	Latitude (°S)	Name	Run-up (m)	Inundation distance (m)	Comment	Quality
9/17/07 17:00	101.43793	2.96731	Ipuh (Retak Ilir)	1.8	47	A maximum run-up, did not exceed	***
9/17/07 17:45	101.51154	3.07636	South Ipuh	2.2	93	Very clear inundation line. Energetic, large driftwood moved around	*****
9/17/07 15:00	101.52643	3.10175	Air Rami	1.8	172	Witness described run-up	*****
9/17/07 16:30	101.52225	3.11234	South Air Rami	2.0	150	Estimate only. Evidence of inundation across island, lagoon	***
9/17/07 12:00	101.66450	3.27505	Pantai Indah	1.9	50	Very clear run-up mark	*****
9/17/07 11:15	101.72724	3.32086	Karang Pulau	3.3	45	Very clear run-up mark	*****
9/17/07 9:00	101.90155	3.42991	Serangai	3.5 to 5.0	500	Sustained flow at 3.5 m. Splash over cliff top to 5.0 m, possibly more. Wave described as breaking bore	***
9/17/07 8:30	101.90923	3.43523	Serangai 2	3.0	140	Estimate only	**
9/15/07 17:15	102.03394	3.53072	Lais 2	3.0	35	Clear run-up mark	*****
9/15/07 16:45	102.03592	3.53163	Lais 1	3.9	30	Steep cliff coast, inundated over sea wall	*****
9/15/07 11:15	102.26022	3.78209	Bengkulu 4	1.4	151	Clear run-up mark. Houses flooded to 40 cm	*****
9/15/07 10:45	102.25414	3.78538	Bengkulu 3	1.7	130	Inundated over seawall. Did not move steel pipes	****
9/15/07 10:00	102.25116	3.78549	Bengkulu 2	1.4	0	Located in fishing port. Run-up on a vertical wall	*****
9/15/07 9:00	102.25028	3.79666	Bengkulu	1.4	40	A maximum value. No witness, run-up line not clear	***
9/18/07 11:45	102.30352	3.88556	Port North	1.2	64	Clear mark identified by witness	*****
9/18/07 8:45	102.27493	3.90038	Port South	0.9 to 1.7	90	No witness. Lower value is elevation at debris line. Larger value is needed to overtop beach berm	***
9/16/07 10:00	102.51948	4.14423	Pasar Seluma	1.3 to 2.0	100	No direct witness. Run-up mark unclear	**
9/16/07 12:30	102.79430	4.35269	Muara Maras	0.9 to 1.7	281	Clear inundation. Some tsunami damage. Flooded across road into swampy area	*****
9/16/07 14:00	102.89955	4.47753	Pasar Bawah Manna	3.5	56	Slow inundation, overtopped sea wall	*****
9/16/07 16:30	103.12446	4.58738	Teluk Biringin	1.4	20	Did not overtop beach berm	*****

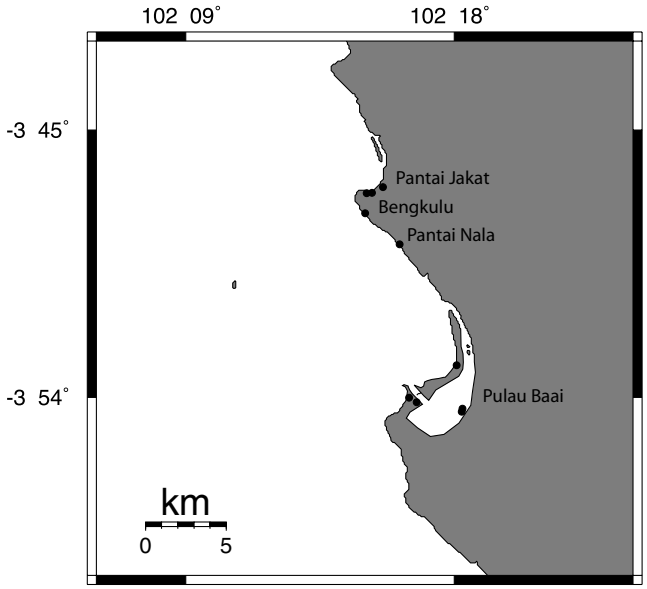

Figure 4. Locations surveyed near Bengkulu.

The elevation of the ground level relative to sea level at the time of the tsunami was measured to be 0.85 m. However, the wave height necessary to overtop the beach berm at this location is at least 1.65 m. The inundation extended to 90 m inland. It was evident that the flooding was not very energetic or erosive because there were no clear signs of large-scale erosion across the berm ridge. Also a small bench constructed from driftwood located on the crest of the berm was intact and undisturbed.

At a small town just north of the harbour, local residents reported that the tsunami first arrived 30 min after the earthquake. A local shopkeeper, whose store was located directly on the beach front, did not evacuate with other residents after observing the first wave. He reported that there were a total of 4 surges separated by 1 hr with the 4th surge being the largest.

2.2 Southern region

A broad, low lying coastal plain with an extensive inland lagoon system, fed by numerous rivers, characterizes the region immediately south of Bengkulu. The main coastal highway lies 20 km inland making direct access to the coast difficult and time consuming; thus, only one point was surveyed near the centre of this region at Pantai Pasar Seluma. It was interesting to note that unreinforced brick buildings similar to those which suffered severe damage to the north of Bengkulu were completely unaffected by the earthquake in the southern region. The local residents felt the ground shaking but did not report any damaged buildings.

At Pantai Pasar Seluma, one eyewitness reported that the water first receded, approximately 1.5 hr after the earthquake, indicative of a leading depression N-wave (LDN) (Tadepalli & Synolakis 1994). The sea level stayed out for 15–20 min before returning. The witness observed this while others in the area evacuated ahead of him. Upon noticing the waters rising again, he then fled the area on his motorbike. The strongest surges were around 8 p.m. according to the witness and surges were observed moving up a nearby river up to 2 km inland. Inspection of the beach did not show evidence of a large or energetic tsunami. The dunes were intact with no signs of erosion. There was evidence that the tsunami inundated the roadway access that cut between the dunes and the witness confirmed this. The elevation at the inland extent of inundation was 1.5 m with a minimum of 50 m of inundation.

Continuing south, the highway returns to the shoreline near the village of Muara Maras. Here, the tsunami inundation was severe with many witnesses and small-scale damage to houses near the shoreline. Large driftwood logs were transported from the beach and deposited in the streets of the village. An inundation debris line was clearly seen in the forest behind the village with a second debris line observed another 20 m inland of this line. Water levels noted on buildings were in the range of 0.5–1.0 m. An administrative office, which was located on the waterfront, was inundated but suffered no damage. Notably the glass windows in the structure were not damaged. We use the lower level of the window glass as an upper limit for the flow depth at this location.

According to residents, the sea first receded at approximately 6:30 p.m. with the first positive wave arriving at approximately 7:00 p.m. This was followed by a shorter second withdrawal closely followed (5–10 min) by the second positive surge. The second positive surge overtopped the beach berm, which at the time of the tsunami was approximately 1.7 m above sea level. This was followed again by another withdrawal, which residents reported as not particularly large, i.e. as not exceeding more than 20 m from the 'normal' shoreline line. The third elevation wave was the largest and flooded across the beach berm, through the village, across the highway and up to 280 m from the shoreline.

Considering the inundation, the damage at Muara Maras was not severe. The houses located close to shore were uniformly flooded, however only five structures were damaged. The types of structures damaged were limited to walls built of unreinforced rock, especially those oriented perpendicular to the direction of tsunami travel. It is likely that the tsunami was just large enough to overtop the berm and flood the village, which sits at an elevation below the crest of the beach berm.

Two additional sites were surveyed south of Muara Maras, Pasar Bawah Manna and Teluk Biringin. At Pasar Bawah Manna, the survey site was located in a sheltered area behind a headland. Along the narrow beach, there was evidence that the tsunami overtopped the sea wall, based on the large amount of debris deposited there. The tide-corrected elevation to the debris line was 3.5 m. Eyewitnesses interviewed here said the earthquake occurred during the time of the afternoon prayers, at which time they evacuated to higher ground. At approximately 8:30 p.m., one witness returned alone and observed by torchlight that the water had receded. The inundation was 'slow and even and peaked at approximately 9 p.m'. The run-up measured here was considerably higher than at Muara Maras to the north and Teluk Biringin to the south. At the southernmost survey site, it was clear that the tsunami did not overtop the beach berm. One local resident who lived on the beach noted that the debris line from previous high tides was raised to a higher level by the tsunami. This elevation was measured to be 1.4 m corrected for tide. If overtopping had occurred, we would have expected much more debris behind the berm.

2.3 Northern section

The region north of Bengkulu experienced the brunt of the earthquake and tsunami. Starting at Lais, there was evidence of severe ground shaking which included large ground fissures and cracks as well as severely damaged or destroyed buildings including the local school. A continuous GPS receiving station used to measure ground level changes was installed at the school in 2006. The station was not damaged, however the intensity of the ground shaking did

cause a rusted mounting bracket for the data transmission antenna to break. During the survey, the bracket was repaired so that the data could be downloaded for analysis.

At Lais, the tsunami run-up was measured to be between 2 and 4 m when corrected for tide. However, it produced no damaging effects as near-shore cliffs with heights of the order of 10–20 m front the coastline. The highway and the local towns are all located at tsunami-safe elevations. A clear run-up mark of 3.9 m was measured on one steep cliff. This was consistent with another location 200 m along the coast where another very clear inundation line was measured at 3 m at a distance of 35 m from shore. Driving north of Lais, the coastal cliffs are not as prominent and the highway drops down to near sea level. In this area, tsunami inundation across the highway was evident and extended up to several hundred meters inland but was not measured directly due to time constraints.

At the next location to the north at Serangai Village, a small cluster of houses situated on lowlands between coastal cliffs, a local resident, who sought refuge at the top of the cliffs, observed the tsunami. Eyewitnesses reported that the water first receded approximately 20 min after the earthquake, then returned 20 min later. All along the sea cliff up to elevations of 5–8 m, the effect of tsunami overtopping was observed in the form of vegetation that had been bent backward due to the overland flow. One witness suggested that this was caused by a large splash that occurred when the advancing tsunami wave front struck the steep cliff-face. The same witness indicated the level on the sea cliff that he thought best represented the sustained flow depth of the overall tsunami wave. This elevation was measured at 3.5 m after correction for tide.

At this location, several houses were destroyed by the wave. At an undamaged house located approximately 200 m inland the tsunami flooded some 1-m deep. Residents indicated that the tsunami continued inland until it reached the river. Inspection of aerial imagery of this area shows this distance to be on the order of 500 m.

The tsunami was clearly observed at the next two locations northward, Karang Pulau (Cliff Island) and Pantai Indah (Beautiful Beach). At Karang Pulau, the witnesses reported that the first surge was the largest and arrived 25 min after the earthquake. Between the first and second wave, there was an interval of 25 min. One witness reported that there were up to seven surges with 10–15 min between crests. Of these, the first was the largest, followed by three smaller surges with the wave height diminishing from the fifth crest onward. This witness reported hearing a 'Boom-Boom-Boom' sound as the tsunami approached and described the initial advancing wave front as being similar to a bore. The inundation at Karang Pulau was clearly identified by the presence of a debris line wedged into the coastal bluff. Corrected run-up at Karang Pulau was measured at 3.3 m. Approximately 10 km north at Pantai Indah, an obvious debris line indicated the extent of tsunami run-up; however, the inundation was not observed directly. Fearing a large tsunami after the powerful earthquake, the residents evacuated to higher ground upon observing a withdrawal of the sea level. Run-up measured at Pantai Indah was 1.9 m at 50 m inundation.

Four data points were collected in vicinity of Air Rami and Ipuh. South of Air Rami, there is a headland with a sheltered beach to the north. Here, a 50-m wide lagoon backs a beachfront forest. Tsunami inundation traces were observed on the landward bank of the lagoon, approximately 300 m from the shoreline. Locals confirmed that the tsunami overtopped the beach berm, crossed the lagoon and deposited a large log next to a waterfront eatery (a 'warung'). Further north, at Air Rami, there was clear evidence of tsunami run-up and we were also able to obtain concomitant eyewitness accounts. A debris line was confirmed by an eyewitness and measured at 1.8 m after accounting for the tide. Accounts of the wave behaviour claim there were 10 separate surges with the fifth wave being the largest. The witnesses also reported a 15- to 20-min interval between waves with the first wave arriving at approximately 8 p.m. This however appears unlikely, as it is too late relative to the source location and other accounts of the wave arrival from other sites nearby. At this location, swell waves were observed to be breaking a great distance offshore. Inspection of the nautical charts for this area indicates the presence of offshore shoals, which could explain the later arrival and large number of wave peaks.

Continuing northward, just south of Ipuh, a very clear inundation line was observed in a coastal forest. Many large driftwood logs were picked up by the tsunami and deposited further inland. The run-up was measured to be 2.2 m with an inundation distance of 93 m. Several impact scars from floating debris (the large logs) were observed on the tree trunks and uniformly indicated a flow depth on the order of 1 m close to the beach that tapered towards the maximum inundation distance.

Finally, the northernmost data point was recorded north of the town of Ipuh (Retak Ilir coast). At this location, there was evidence of liquefaction and small-scale ground failures in the mostly sandy soil. It was unclear if the tsunami overtopped the beach berm and spilled into the partially dry lagoon behind. One local resident who was working on a construction project nearby claimed that the beach berm was not overtopped but the lagoon was flooded via a river mouth inlet located 200 m to the north. This would provide a satisfactory explanation for the presence of stranded debris in the dry low lying area behind the beach while there was still a significant amount of driftwood remaining on the beach. Had over topping occurred, we would have expected much more debris behind the berm. An inundation line was identified on the beach face and measured to be 1.8 m corrected for tide.

2.4 Tsunami awareness and evacuation practices

The level of tsunami awareness among the local population was nothing short of admirable. In simple terms, the population self-evacuated, and this must be the dominant factor which prevented any deaths or injuries directly related to the tsunami. The population must be commended for their responsible and effective behaviour. Indeed, at several sites, there were no direct observations of the tsunami wave for the simple reason that everyone evacuated after either feeling the strong, long-lasting ground shaking or if they were not entirely convinced of the potential danger after seeing the sea level begin to withdraw. At a few locations, there was an excellent direct observation from witnesses who had evacuated to high ground but still had a clear view of the sea. At other locations, men evacuated their families initially and then returned to monitor the situation. In no instances, however, there were any reports of injuries or deaths directly related to the tsunami. There was no discussion amongst witnesses and residents of the need for an official warning system, as every one seemed to fully understand the association between strong earthquakes and the potential for a deadly tsunami. This underscores the need for education in tsunami preparedness (Synolakis & Kong 2006) and is in contrast to observations of the 2006 East Java tsunami, which claimed at least 600 lives (Fritz *et al.* 2007). Note however that the latter was clearly a so-called 'tsunami earthquake', featuring a slow-rupturing source deficient in high-frequency seismic energy, and thus contributing only deceptively weak ground shaking in the frequency bands most detectable by

human beings (Kanamori 1972; Newman & Okal 1998; Okal 2007). Such treacherous events have most often resulted in significant loss of life (e.g., Sanriku, Japan, 1896 June 15), and constitute a major challenge for near-field tsunami warning.

3 NUMERICAL MODELLING OF THE BENGKULU TSUNAMI

Following a large offshore earthquake, there is always a need to rapidly assess the tsunamigenic potential of the event. Such analyses provide information critical to the decision-making process for warning or evacuating areas located more than a few hours of tsunami travel time from the source region, as well as planning for emergency relief. Although near source areas are unlikely to benefit from this information (due to the rapid onset of the tsunami), it is still important to assess the size and extent of damaging tsunami effects in the near field for the purposes of rescue and relief operations in remote or inaccessible areas, or for guidance to post-event reconnaissance. This study compares various methods for evaluation and modelling of tsunami effects in both the near and far fields, in terms of their relative accuracies and the time they require.

3.1 Tsunami modelling method

To simulate the tsunami generated by an earthquake source, we used the model MOST—Method of Splitting Tsunami (Titov & Gonzalez 1997; Titov & Synolakis 1998; Titov *et al*. 2005), a fully validated and benchmarked hydrodynamic model used for operational tsunami propagation and inundation assessments. MOST uses the final dislocation field from a seismic deformation model to initialize hydrodynamic computations, taking into account the on-land crustal deformation from the earthquake when computing the wave evolution and run-up onto dry land.

In order to perform reliable modelling of tsunami inundation and run-up, a detailed model of near-shore bathymetry and coastal topography is necessary. For the modelling described here, we used a data set generated by digitizing the available nautical charts and combining this data with publicly available deep-water bathymetry and near-shore topography.[1] To accurately reflect the coastal topography in the areas of interest, the data were compared to available aerial imagery and manually adjusted, if necessary, using near-shore topographic profiles measured during the field survey.

Four different computational grids were used for studying the tsunami propagation. To simulate the near-field tsunami run-up, a system of three telescoping rectangular computational grids in geophysical coordinates was used. This allows for an efficient numerical solution over an area that covers the region directly affected by the earthquake dislocation and tsunami. The wider geographic area was modelled with 1200 m and 600 m coarser outer grids, while the onshore run-up with a 200-m innermost grid. This resolution was used to avoid the well-known underestimation issues that plague threshold models that stop the calculation at some offshore depth (Synolakis & Bernard 2006). While 200-m grids are on the borderline of being too coarse, limitations in the available source data for creating the computational grids prevented us from using higher-resolution grids; interpolating within grids may improve numerical accuracy but does not necessarily improve geophysical realism. In this modelling framework, any initial condition can be assigned onto the coarser outer grid with the results propagated through the system of nested grids with the full run-up computation carried out in the finest near-shore grid. For the ocean-wide modelling, a relatively coarse (4 arcmin or ∼7400 m) grid was used, which is sufficient to resolve the tsunami dynamics in deep water (Gica *et al.* 2007).

3.2 Tsunami source models

Within minutes of an earthquake, the first estimates of the magnitude coupled with historical precedent allow for an initial assessment of the likelihood of a tsunami. Simultaneously available information on the earthquake location allows for a rapid estimate of tsunami wave arrival times at locations potentially in harms way. This is the information provided in the initial messages disseminated by the Pacific and West Coast-Alaska Tsunami Warning Centers (PTWC and WCATWC), which generally give no indication of the size or destructive potential of the tsunami that may have been generated. As time passes and seismic data is processed, more detailed versions of the source model emerge, generally within the time frame of a few hours to several days. At even later times, i.e. weeks or months, field investigations and instrumental data further constrain the seismic source.

In the present study, four different variations (Fig. 5) of the vertical sea-floor deformation caused by the earthquake were used to initialize the tsunami simulation. The first tsunami source is the simplest and most readily available – a single rectangular fault plane with constant slip. In this case, the fault parameters are inferred from an estimate of the seismic moment (equivalent to the long-period magnitude of the earthquake), and a general understanding of the local seismotectonic framework. The latter provides the orientation of the fault and a possible limitation on the maximum depth of the seismic zone (to constrain fault width). Scaling laws (Geller 1976) are used to convert a seismic moment into explicit fault parameters, such as seismic slip, fault length and fault width. Their use assumes that the earthquake does not feature an anomalous behaviour (e.g. excessive source slowness such as in the case of so-called 'tsunami earthquakes'), which can be verified through the use of real-time tests (e.g. the computation of the parameter Θ [Weinstein & Okal 2005]). The dip and slip angles of the focal mechanism are taken from representative focal mechanisms published as part of the Global Centroid Moment tensor inversion project. In the present study, we used $\delta = 10^{\circ}$ and $\lambda = 90^{\circ}$, the latter expressing total slip partitioning of the oblique convergence, between the SSZ and the strike-slip Sumatra fault inland. This model of source can be obtained as soon as the 'real-time' estimate of the seismic characteristics of the event are available, in practice 15–30 min after origin time (e.g. Weinstein & Okal 2005). Once the model is defined, the resulting static vertical deformation is computed using the algorithm of Mansinha & Smylie (1971). The rectangular source (RS) used here has fault dimensions of 190 by 95 km, with a uniform slip of 5.6 m. The fault plane extends northwest from the epicentre. The resulting field of static vertical deformation is shown in Fig. 5(a).

The next type of initial condition retains the simple rectangular fault idea, but allows for more flexibility in defining the source

[1] 1:250000-scale nautical charts from the Indonesian hydrographic service were scanned and geo-referenced to lat/long coordinates using the appropriate datum (UTM48-S, Batavia) and spheroid (Bessel 1841), as specified on the charts. All contours, soundings and land elevations on the charts were then digitized by hand. These data were then combined with the SRTM30_PLUS data set (http://topex.ucsd.edu) to generate a combined map containing near and offshore bathymetry and coastal topography. The combined data set was then interpolated to a 200-m grid in lat/long coordinates in the WGS84 projection.

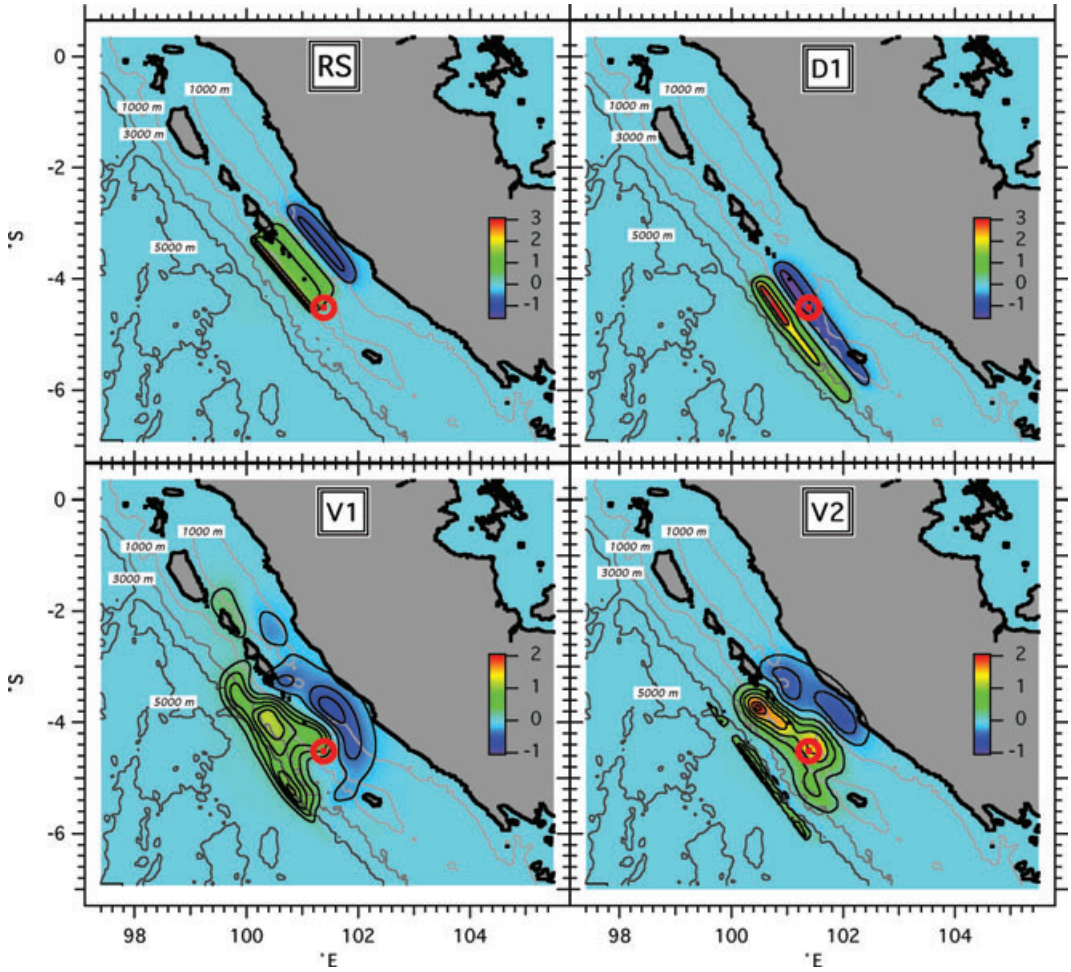

Figure 5. Computed vertical uplift from each of the four scenarios. Colour scale units are in metres. The red bull's-eye is the location of the USGS epicentre.

model. A pre-computed tsunami propagation database is used in combination with real-time sea level data recorded by one or more DART buoys (Bernard *et al.* 2006; Bernard & Titov 2007). Results using this method are available as a predictive or real-time tsunami forecast tool generally within 1–3 hr after the event, depending on the location of the DART buoy(s) relative to the earthquake. In this forecast-oriented modelling framework, the linear, deep-water phase of tsunami propagation has been pre-computed and stored in a database comprised of the full tsunami wave propagation estimated from a series of 100-km long by 50-km wide fault segments with 1 m of uniform slip (i.e. equivalent to an earthquake of $M_w = 7.5$). The source segments are arranged in parallel rows situated along the earth's major subduction zones as in Wei *et al.* (2008). Wave propagation patterns originating from these unit sources are linearly combined to construct more complicated sources (Bernard 2005). This allows for the reconstruction of a specific earthquake event either by approximating the solution with available preliminary earthquake data or by inverting real-time sea level data via a process of selecting a combination of unit sources based on tsunami arrival time at the DART station(s) in conjunction with a least-squares approach providing a 'best fit' to the observed DART signal(s).

On 2007 September 12, DART 23401 located at 8.9°N and 88.5°E (see Fig. 10) was in operation in the Indian Ocean, approximately 2.5 hr in tsunami travel time from the earthquake epicentre. Data recorded by this instrument and transmitted in real time was used to constrain the earthquake source and initialize the tsunami model. The DART inverted source (D1) used three fault segments from the database, and assigned slip amounts of 8.7, 5.6 and 3.9 m, respectively, for a total $M_w = 8.3$. The resultant surface deformation generated by the (D1) source is shown in Fig. 5(b). While the detailed run-up for this source was not computed in real time, the NOAA Center for Tsunami Research (NCTR) made the far-field results available to the public within 5 hr of the earthquake.

The third source used here is the first of two detailed earthquake models that invert seismic waveforms in addition to other data sources (i.e. GPS and direct observations) to determine the slip distribution and subsequent seafloor deformation. Since these models require significantly more time to prepare as compared to the first two cases, they are not available for real-time warning guidance. Source V1 (Fig. 5c) uses only seismic wave data and was determined through the inversion of 20 teleseismic broad-band *P* waveforms, 13 broad-band SH waveforms and 38 long period surface waves. The waveforms were converted to ground displacement by removing the instrument response and then used to constrain the slip history based on a finite fault inverse algorithm (Ji *et al* 2002). For this source, the hypocentre as defined by the U.S. Geological Survey (USGS) (4.52°S, 101.38°E) was used and the fault planes were defined using information from the QUICK moment tensor solution of the Global CMT Project and the assumed orientation of the trench axis. The seismic moment release from this scenario was 5.05×10^{28} dyne-cm ($M_w = 8.47$) using a 1-D crustal model

interpolated from CRUST2.0 (Bassin *et al.* 2000). The resulting source model gives the faulting parameters for 308 individual fault segments along the rupture plane.

The fourth deformation model (V2; Fig. 5d) incorporates a wider variety of data and was derived through the combination of seismic wave inversion and measurements of coseismic crustal deformation as recorded by an array of GPS stations located in the source region as well as direct human observations of ground deformation during post-event reconnaissance surveys. This deformation model was not available until several weeks after the event; its details are described in Konca *et al.* (2008).

3.3 Model results – near field

Figure 6(a) compares the computed run-up to the measured field data for the RS and D1 sources while Fig. 6(b) compares the results for the V1 and V2 sources. While the RS source produces a good fit to the field data, the D1 source over predicts the measured run-up. The two variable source models on the other hand, generally underpredict the measured run-up heights. In the southern section of the modelling region, the RS, V1 and V2 sources produce very similar results. Towards the north, however, the run-up from the V1 and V2 cases fall off to levels well below the measured data. The D1 source agrees with measured data in the northern one-third of the field data locations, but over-predicts the measured values south of 3.2°. The over estimation of the tsunami run-up in the southern region from the D1 scenario is attributed to the use of the southernmost fault segment. Seismological and geological data suggest, however, that this region did not experience a significant rupture or associated coseismic deformation.

As seen in Table 2, the maximum values of uplift and subsidence as predicted by the V1 and V2 sources are approximately half those in the RS and D1 models. For this reason, we performed additional simulations where the V1 and V2 source models were scaled up by a factor of 2. The models were re-run and the result plotted in Fig. 7 which shows that the scaled up deformation fields produce a better fit to the observed data.

In addition to the run-up results, computed wave height time series data were extracted at four locations along the coast from the simulations of the scenarios which best match the measured run-up data – RS, D1, V1 × 2 and V2 × 2 (Fig. 8). The time series show an initial withdrawal of the sea level, beginning immediately after the earthquake for the RS, V1 and V2 cases. However, in the D1 scenario, the initial withdrawal does not appear until approximately 40 min after the earthquake. For the northern sites, Air Rami and Serangai, the first wave is the largest of the series for three of the four source models and is generally characterized as a sharp rise in the water level following the initial withdrawal. Eyewitness accounts at Serangai described an initial withdrawal suggestive of an LDN (Tadepalli & Synolakis 1994) starting shortly after the earthquake (∼20 min) with the first wave arriving 20 min after that. The witnesses reported that the first elevation wave was the largest and arrived as a steep faced bore, which caused a strong splash upon impact with the coastal bluffs. In terms of timing and character of the waves, the V2 × 2 and the RS model agree best with these observations. The D1 source shows a similar record, however, somewhat delayed relative to the witnesses'

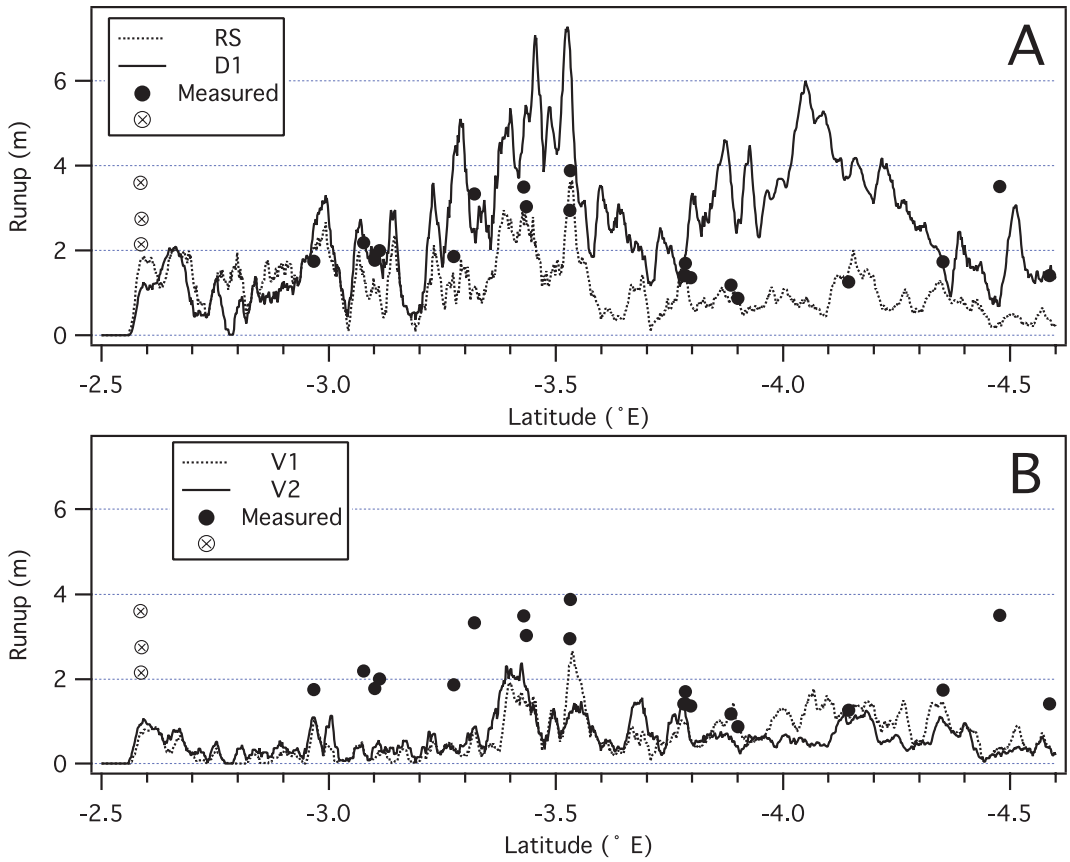

Figure 6. Computed tsunami run up from MOST for the four scenarios compared to measured field data.

Table 2. Seismic source parameters for the four earthquake models tested.

Case	No. of sub faults	L (km)	W (km)	Slip (m)	M_o (dyne-cm)	M_w	Max (Pos)	Max (Neg)
RS	1	190	90	5.6	5.0×10^{28}	8.4	+2.6 m	−1.1 m
		100	50	8.7				
D1	3	100	50	5.6	3.2×10^{28}	8.3	+3.1 m	−2.1 m
		100	50	3.9				
V1	308	–	–	–	5.0×10^{28}	8.47	+1.2 m	−0.7 m
V2	n/a	–	–	–	5.15×10^{28}		+1.5 m	−0.5 m

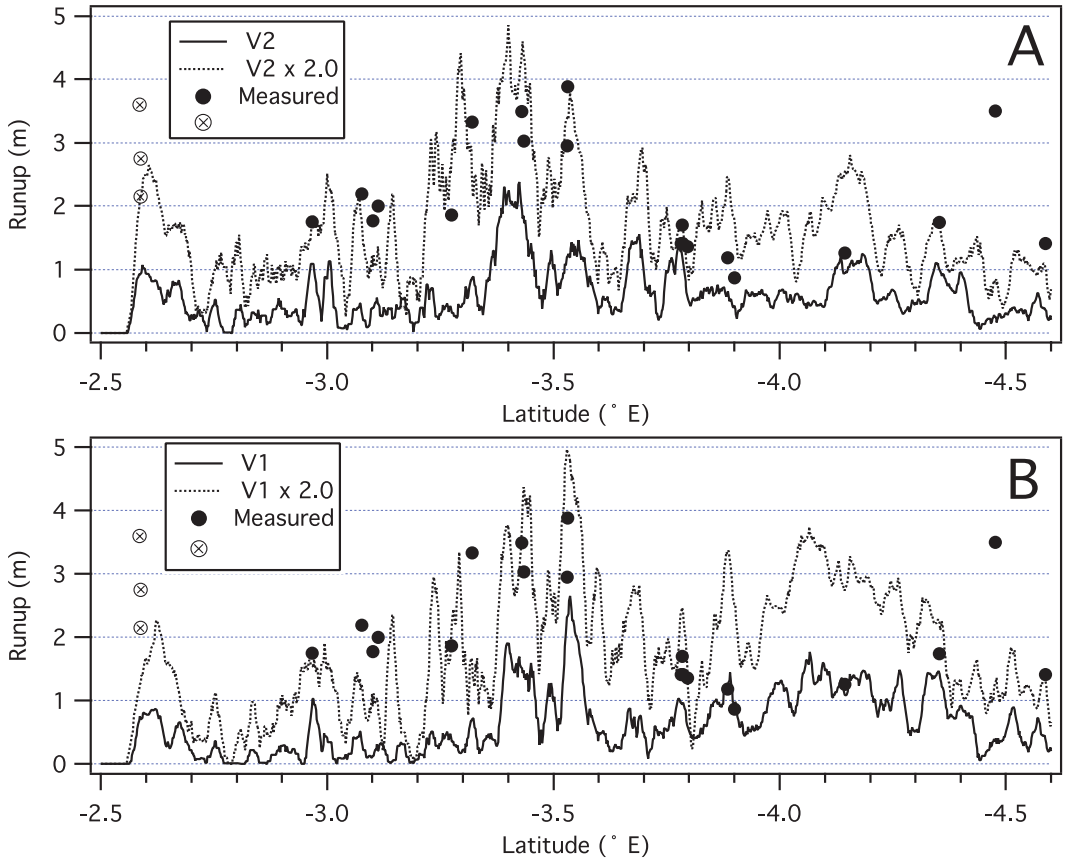

Figure 7. Results of the scaled V1 and V2 sources compared to the measured field data.

description of the event. The V1 × 2 model shows two positive surges of roughly equal height separated by approximately 20 min; however, witnesses in the area did not report wave activity of this sort.

At Bengkulu, the model results suggest four positive surges in the initial 2.5 hr after the earthquake. Local residents reported three to four surges as well, particularly at Pantai Jakat, located just north of the Bengkulu fishing port. For the V2 × 2 and RS cases, the model suggests that the third surge was the largest, as reported by witnesses. The V1 × 2 and D1 source models also suggest a third surge that is at least as large as the first or second waves. At Muara Maras, the V2 × 2 and RS models feature three surges as well, however of smaller amplitude and longer period than at Bengkulu. Similar to witness reports, the models predict a larger third surge, peaking 2.2–2.4 hr after the earthquake. In the V2 × 2 model, the third surge is distinctly larger than the preceding two pulses and appears to fit the witness reports the best. The arrival time of the first positive surge at Muara Maras agrees in general to witness reports (approx 1 hr after the earthquake). Neither the RS nor the V2 × 2 model, however, predict an initial withdrawal of sea level as suggested by the other models and reported by the eyewitnesses.

3.4 Model results—far field

The MOST model was then used to examine the far-field signature of the tsunami by comparing the model results to measured water levels of the tsunami at DART 23401. The four deformation scenarios giving the best fit to the near-field run-up data (RS, D1, V1 × 2 and V2 × 2) were used to initialize the numerical model. Fig. 9 shows the radiation pattern of tsunami wave heights across the Indian Ocean basin for the four source models, while Fig. 10 compares the computed and recorded water levels at DART 23401. It is clear that both the RS and the D1 source models provide a good fit to the measured water levels. The RS source in particular matches the DART data quite well. In contrast, the scaled up V1 × 2 and V2 × 2 sources do not provide as good a fit to the data. Both models over predict the first wave amplitude and the arrival time by approximately 15 min.

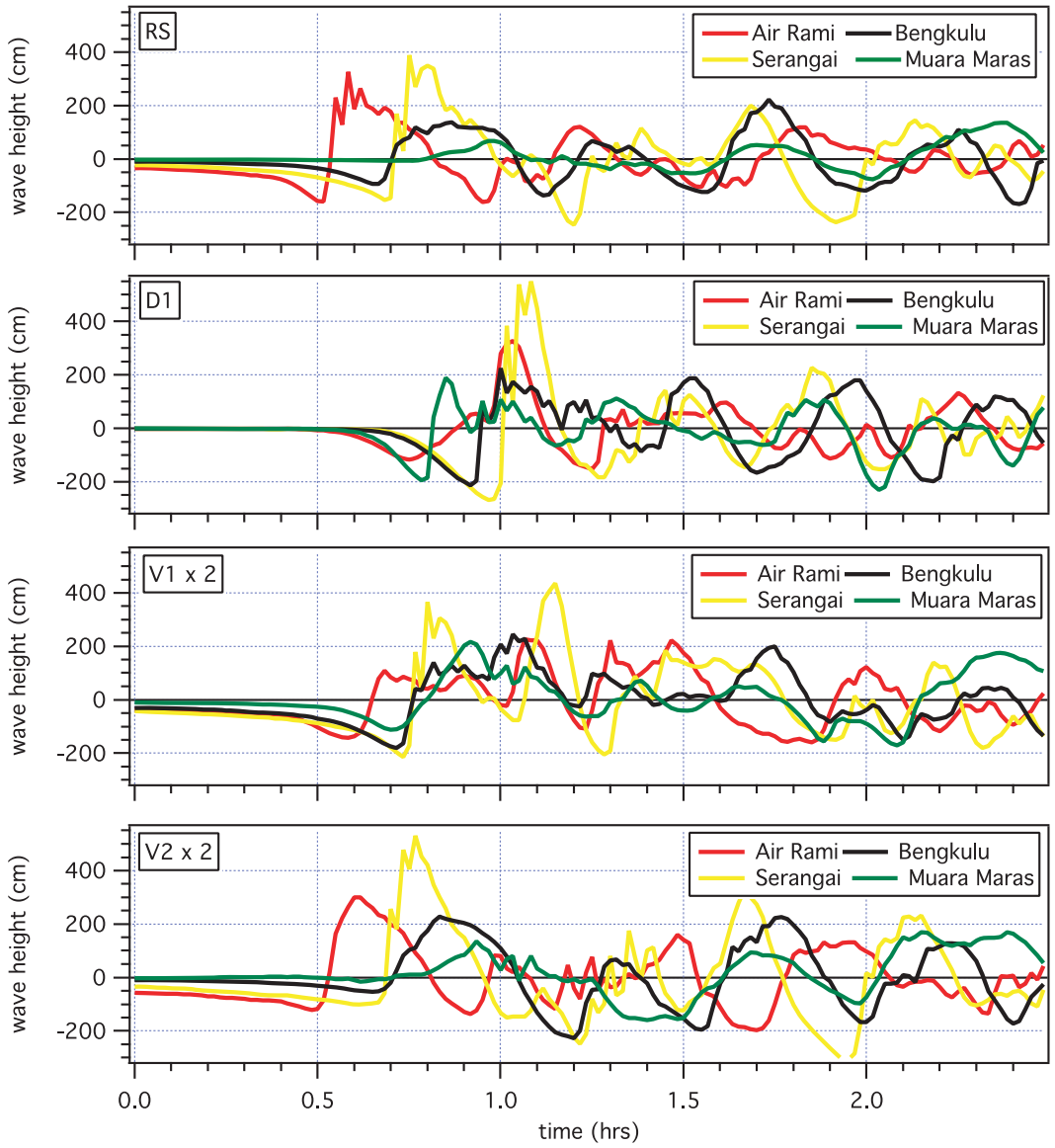

Figure 8. Plots of wave height versus time for four locations along the coast for each of the four scenarios.

4 DISCUSSION AND CONCLUSIONS

Of the four scenarios tested here, the simple RS, uniform slip model produced the best overall fit to the measured field data and to the measured water levels at the DART buoy. This is notable since this simple model is the most readily available in terms of scenario forecasting in the hours immediately following the earthquake. In this respect, we note that recent research (Weinstein & Lundgren 2008) has demonstrated the feasibility of obtaining acceptable source tomographic models based on teleseismic *P* waves, potentially within 1 hr of origin time if using a clustered network of processors. Such a timeframe would make available improved source models for numerical simulations in the context of real-time tsunami warning in the far field.

Source D1 has a reasonable correlation with the field data, but generally over predicted the measured run-up (Fig. 5b). Moreover, comparison of computed wave heights from this source at the DART location with sea level observations beyond the time window of the first wave period used in the source inversion does not show as good an agreement as that of the RS source, particularly in the 3.25- to 4-hr time interval. This feature can be ascribed to the fixed locations of the sources inside the NCTR propagation database, but also illustrates the importance of using both seismic and water-level data in real time as independent measurements of the tsunami.

The results from the V1 and V2 models are less straightforward. The original versions of these sources require a two-fold increase in the vertical deformation in order to accurately reproduce the surveyed run-up, but these same scaled-up sources then over-predict the wave heights at DART 23401. This situation, in which the composite fault models provide a poorer fit than does the uniform slip source to the complete data set of wave amplitudes (including both near- and far-field), is in contrast to the case of the August 2007 Peruvian earthquake and tsunami, for which Fritz *et al.* (2008) showed that the composite model featuring a distributed slip pattern was required to match the results of their survey. We thus caution against drawing universal conclusions as to the relative effectiveness, for the purpose of predicting or explaining near-field inundation, of the simple, uniform source models easily obtained

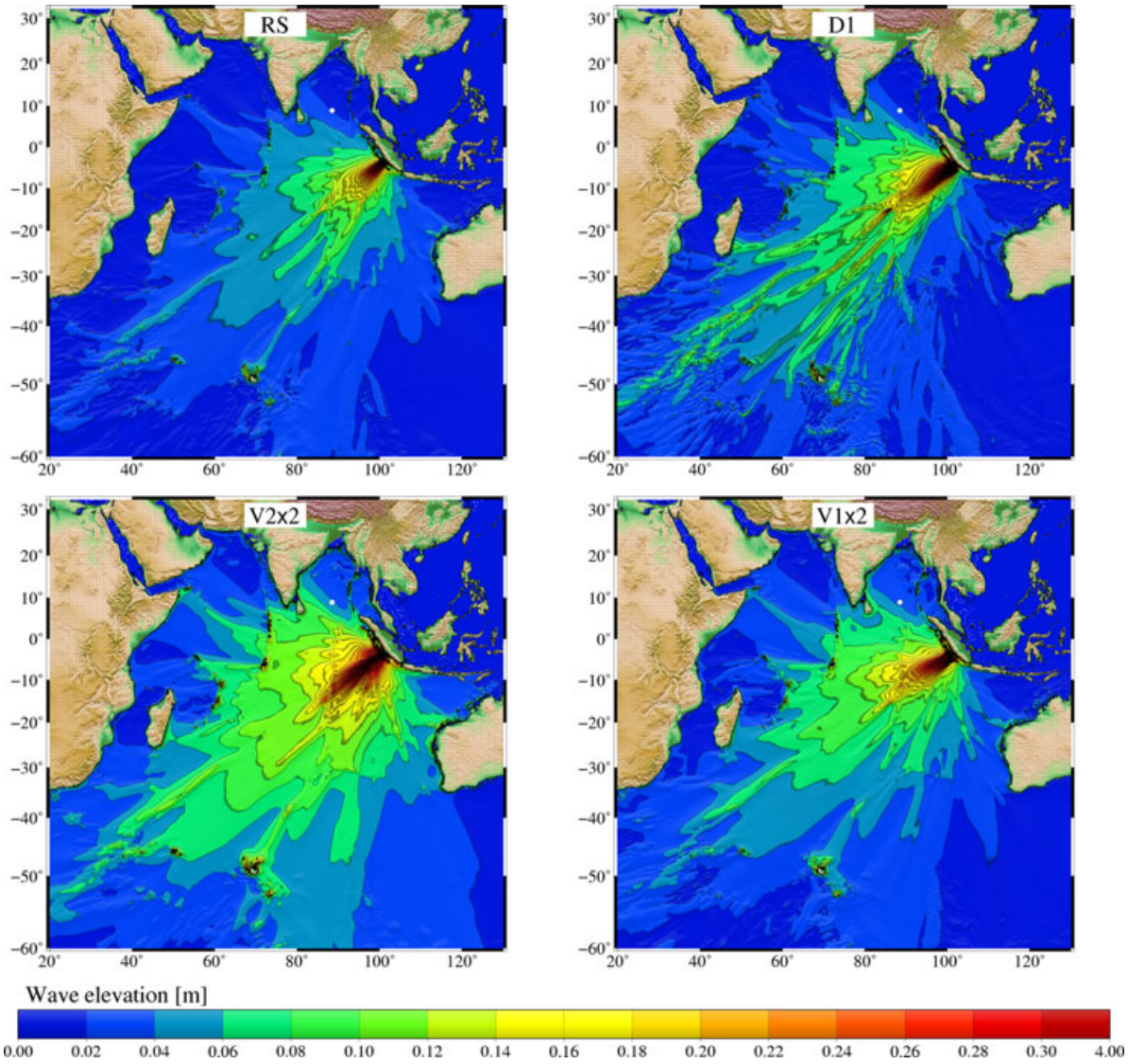

Figure 9. Distribution of maximum wave elevation computed from four deformation scenarios, RS, D1, V1 × 2 and V2 × 2. The location of DART 23401 is indicated in each figure by the white dot.

in quasi-real time, and of the composite fault descriptions which become available following the event at present routinely in a matter of days and weeks, and potentially within an hour or so, when the algorithm suggested by Weinstein & Lundgren (2008) can be implemented on faster processors. While there can be no doubt that the timely identification of such source properties as a slow rupture velocity is beneficial in the context of tsunami warning, especially in the near field, it is clear that further research remains necessary to unravel the added value of such improved characterizations of the seismic source, as related to their contributions to tsunami amplitudes and hazard, especially in the far field.

Despite the numerous advantages of complex fault solutions, time constraints intrinsic to the operation of a tsunami forecast system prevent their use in a time sensitive forecast or warning environment. In most cases, insufficient seismic data is available immediately following an earthquake event and it is impractical for tsunami forecasters to attempt an elaborate seismic inversion of the event. Even on the few occasions in which sufficient and good quality data are available, computation of a forecast requires the simulation of the wave propagation throughout its linear, open ocean regime and non-linear coastal stage which is altogether too time consuming for any forecast or warning purposes.

Also, and in more general terms, the satisfactory performance of the RS model expresses the fundamental low-frequency (and hence long-wavelength) character of the tsunami phenomenon. The generation of the tsunami wave involves the integration of the seismic source over the fault zone, and is essentially less sensitive to its minute details than other, higher-frequency, geophysical fields controlling for example ground motion in frequency bands responsible for shaking and building damage. In the far field, this property was recognized and interpreted by Okal & Synolakis (2008) as reminiscent of Saint-Venant's principle in classical elasticity (Knowles 1966). The present study makes the interesting observation that it may also extend in the near field.

For sea level sensors to provide the best data for source inversion, the sensors should be located along the main beam of the tsunami. It is evident from Fig. 9 that the position of DART 23401 to the side and away from the direction of maximum energy radiation was less than ideal for an accurate inversion of the source. In hindsight, had the DART sensor been centrally along the Sumatra

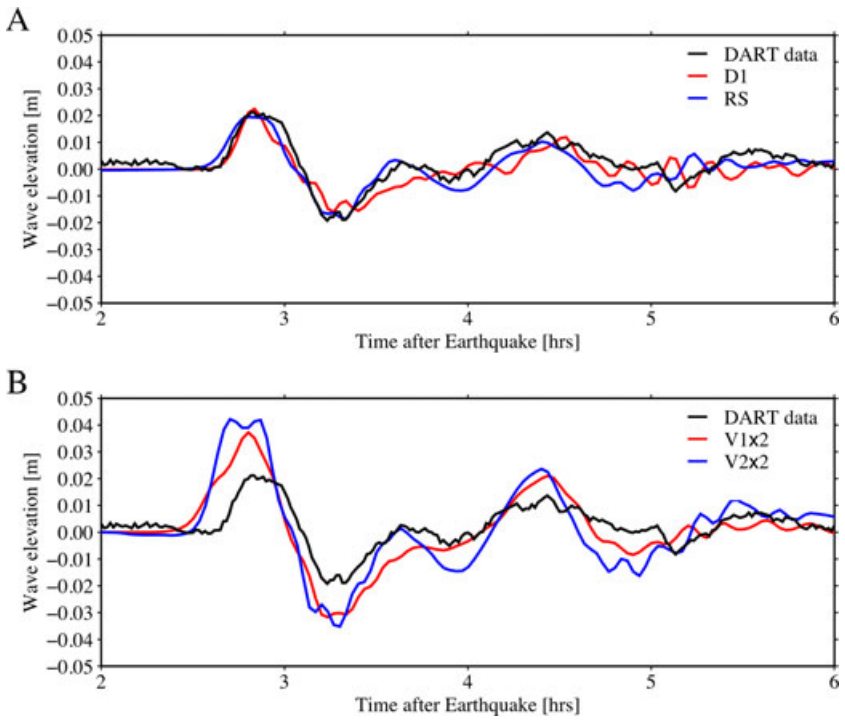

Figure 10. Comparison of model results to measured water levels at DART 23401.

megathrust, it would have been more effective in recording scientifically useful information while providing more accurate forecast and warning information for distant areas throughout the Indian Ocean.

In more analytical terms, the somewhat disappointing performance of the inverted model D1 (illustrated by its lack of clear improvement over RS) stems from the unfavourable geometry of the lone available DART buoy, located in what amounts to a node of radiation of the tsunami wave-field. This leads to performing the inversion under a condition of singularity in the excitation leading to a deterioration of the stability of the inversion.

The real-time, far-field warning capabilities of the DART system in conjunction with a database of pre-computed sources were clearly illustrated during the August 2007 Peru tsunami (Wei *et al.* 2008). In contrast, for communities located close to the tsunami source region, the DART based warning system is impractical due to the very short onset time of the first tsunami waves. During the Bengkulu event, damaging tsunami waves arrived along the coast 30–60 min after the earthquake, 1.5–2 hr before reaching the DART sensor. This reinforces the importance of public education and evacuation planning for tsunami hazard mitigation. Evacuation planning measures should, however, be based on detailed tsunami inundation mapping using realistic tsunami source models calibrated with historical information (e.g. Uslu *et al.* 2007). Threshold modelling as used in McCloskey *et al.* (2007, 2008), to evaluate the tsunami threat from megathrust earthquakes, does not include this pivotal part of inundation hydrodynamic modelling and may not always accurately represent the overall tsunami hazard. In conclusion, we advocate the continued development of warning systems based on real-time tsunami forecasting for the far field in conjunction with public education and evacuation planning (based on detailed inundation modelling) for the near field to be the framework for the realistic and achievable goal of creating tsunami resistant communities worldwide.

ACKNOWLEDGMENTS

We would like to thank Prof. Kerry Sieh and the Seismological Observatory at the California Institute of Technology for financial support of the field survey. Prof. Kusnowidjaja Megawati and Nanyang Technical University provided logistical support in Singapore and hospitality before and after the field survey. A. Konca and C. Ji graciously provided assistance with the seismic models. Aubrey Dugger of GreenInfo Networks provided GIS support. Cyprien Bosserelle of ASR Limited assisted in tsunami modelling. JCB wishes to dedicate this paper to Carla J. Borrero, August 9, 1945 to June 2, 2007.

REFERENCES

Bassin, C., Laske, G. & Masters, G., 2000. The current limits of resolution for surface wave tomography in North America, *EOS Trans. AGU,* **81,** F897.

Bernard, E., 2005. The US National Tsunami Hazard Mitigation Program: a successful state-federal partnership, *Nat. Hazards,* **35,** 5–24.

Bernard, E.N. & Titov, V.V., 2007. Improving tsunami forecast skill using deep ocean observations, *Mar. Tech. Soc. J.,* **40**(3), 23–26.

Bernard, E.N., Mofjeld, H.O., Titov, V.V., Synolakis, C.E. & Gonzalez, F.I., 2006. Tsunami: scientific frontiers, mitigation, forecasting, and policy implications, *Proc. Roy. Soc. London A,* **364** (1845), 1989–2007.

Borrero, J.C., 2005. Field data and satellite imagery of tsunami effects in Banda Aceh, *Science* **308**(5728), doi:10.1126/science.1110957.

Borrero, J.C., Sieh, K., Chlieh, M. & Synolakis, C.E., 2006. Tsunami, inundation modeling for western Sumatra, *Proc. Natl. Acad. Sci.,* **103,** 19 673–19 677.

Chamot-Rooke, N. & Le Pichon, X., 1999. GPS-determined eastward Sundaland motion with respect to Eurasia confirmed by earthquake slip vectors at Sundaland Philippine trenches, *Earth Planet. Sci. Lett.,* **173,** 439–455.

Fritz, H.M. *et al*., 2007. Extreme runup from the 17 July 2006 Java tsunami, *Geophys. Res. Lett.,* **34,** L12602, doi:101029/2007GL029404.

Fritz, H.M., Kalligeris, N., Borrero, J.C., Broncano, P. & Ortega E., 2008. 15 August 2007 Peru tsunami runup observations and modeling, *Geophys. Res. Lett.,* **35,** L10604, doi:10.1029/2008GL033494.

Geist, E., Bilek, S., Arcas, D. & Titov, V.V., 2006. Differences in tsunami generation between the December 26, 2004 and March 28, 2005 Sumatra earthquakes., Earth, Planets, *Space* **58,** 185–193.

Geller, R.J., 1976. Scaling relations for earthquake source parameters and magnitudes, *Bull. Seismol. Soc. Am.,* **66,** 1501–1523.

Gica, E., Teng, M., Liu, P.L.-F, Titov, V.V. & Zhou, H., 2007. Sensitivity analysis of source parameters for earthquake generated distant tsunamis, *J. Waterway Port Coast Ocean Eng.,* **133**(6), 429–441.

Hartnady, C.J.H., & Okal, E.A., 2007. Mentawai tsunami effect at Port Elizabeth, South Africa on 12–14 September 2007, *S. Afr. J. Sci.,* Submitted.

Jackson, L.E., Barrie, J.V., Forbes, D.L., Shaw, J., Mawson, G.K. & Schmidt, M., 2005. Effects of the 26 December 2004 Indian Ocean tsunami in the Republic of Seychelles, *EOS Trans. Am. geophys. Un.,* **86** (52), F6–F7, [abstract].

Ji, C., 2007. Preliminary result of the Sep 12, 2007 Sumatra earthquake, available at http://earthquake.usgs.gov/eqcenter/eqinthenews/2007/us2007hear/finite_fault.php

Ji, C., Wald, D.J. & Helmberger, D.V., 2002. Source description of the 1999 Hector Mine, California earthquake; Part I: wavelet domain inversion theory and resolution analysis, *Bull. Seism. Soc. Am.,* **92**(4), 1192–1207.

Kanamori, H., 1972. Mechanism of tsunami earthquakes, *Phys. Earth Planet. Int.,* **6,** 346–359.

Knowles, J.K., 1966. On St. Venant's principle in the two-dimensional linear theory of elasticity, *Arch. Rat. Mech. Anal.,* **21,** 1–22.

Konca, A.O. *et al*., 2008. Partial rupture of a locked patch of the Sumatra megathrust during the 2007 earthquake sequence, *Nature,* **456,** 631–635.

Mansinha, L. & Smylie, D.E., 1971. The displacement fields of inclined faults, *Bull. Seismol. Soc. Am.,* **61,** 1433–1440.

McAdoo, B.G., Dengler, L., Prasetya, G. & Titov, V.V., 2006. Smong: how an oral history saved thousands on Indonesia's Simeulue Island during the December 2004 and March 2005 tsunamis, *Earthq. Spectra,* **22,** S661–S669.

McClosky, J., Nalbant, S. & Steacy, S., 2005. Indonesian earthquake: Earthquake risk from co-seismic stress, *Nature,* **434,** 291, doi:10.1038/434291a.

McCloskey, J. *et al*., 2007. Near-field propagation of tsunami from megathrust earthquakes, *Geophys. Res. Lett.,* **34,** L14316.

McCloskey, J. *et al*., 2008. Tsunami threat in the Indian Ocean from a future megathrust earthquake west of Sumatra, *Earth Planet. Sci. Lett.,* **265,** 61–81.

Nalbant, S., Steacy, S., Sieh, K., Natawidjaja, D. & McCloskey, J., 2005. Updated earthquake hazard in Sumatra, *Nature,* **435,** 756–757.

Natawidjaja, D.H., Sieh, K., Galetzka, J., Suwargadi, B., Cheng, H., Edwards, L. & Chlieh, M., 2007. Interseismic deformation above the Sunda Megathrust recorded in coral microatolls of the Mentawai islands, West Sumatra, *J. geophys. Res.,* **112,** B02404, doi:10.1029/2006JB004450.

Nettles, M., Ekström, G., Dziewonski, A.M. & Maternovskaya, N., 2005. Source characteristics of the great Sumatra earthquake and its aftershocks, *EOS, Trans. Am. geophys. Un.,* **86**(18), U43A–01, [abstract].

Newman, A.V. & Okal, E.A., 1998. Teleseismic estimates of radiated seismic energy: the E/M_0 discriminant for tsunami earthquakes, *J. geophys. Res.,* **103,** 26 885–26 898.

Okal, E.A., 2007. Performance of robust source estimators for last year's large earthquakes, *EOS, Trans. Am. geophys. Un.,* **88**(52), S44A–01, [abstract].

Okal, E.A. & Synolakis, C.E., 2008. Far-field tsunami hazard from megathrust earthquakes in the Indian Ocean, *Geophys. J. Int.,* **172,** 995–1015.

Ortiz, M. & Bilham, R., 2003. Source area and rupture parameters of the 31 December 1881 $M_w = 7.9$ Car Nicobar earthquake estimated from tsunamis recorded in the Bay of Bengal, *J. geophys. Res.,* **108**(B4), ESE_11, 16.

Pollitz, F., Banerjee, P., Bürgmann, R., Hashimoto, M. & Choosakul, N., 2006. Stress changes along the Sunda trench following the 26 December 2004 Sumatra-Andaman and 28 March 2005 Nias earthquakes, *Geophys. Res. Lett.,* **33,** L06309, doi:10.1029/2005GL024558.

Socquet, A., Vigny, C., Chamot-Rooke, N., Simons, W., Rangin, C. & Ambrosius, B., 2006. India and Sunda plates motion and deformation along their boundary in Myanmardetermined by GPS, *J. geophys. Res.,* **111**(5), B05406, 11.

Stein, S. & Okal, E.A., 2005. Size and speed of the Sumatra earthquake, *Nature,* **434,** 581–582.

Synolakis, C.E. & Bernard, E.N., 2006. Tsunami science before and beyond Boxing Day 2004, *Proc. Roy. Soc. London A.,* **364**(1845), 2231–2265.

Synolakis, C.E. & Kong, L., 2006. Run-up measurements of the December 2004 Indian Ocean Tsunami, *Earthq. Spectra,* **22**(3), 67–91.

Synolakis, C.E. & Okal, E.A., 2005. 1992–2002: Perspective on a decade of post-tsunami surveys, in: *Tsunamis: Case studies and recent developments,* ed. K. Satake, *Adv. Nat. Technol. Hazards,* **23**:1–30.

Tadepalli, S. & Synolakis, C.E., 1994. The run up of N-waves, *Proc. Roy. Soc. London A.,* **445,** 99112.

Titov, V.V. & Gonzalez, F.I., 1997. *Implementation and Testing of the Method of Splitting Tsunami (MOST) National Oceanic and Atmospheric Administration,* Technical Memorandum ERL PMEL-112, Washington, DC.

Titov, V.V. & Synolakis, C.E., 1998. Numerical modeling of tidal wave runup. *J. Waterway Port Coastal Ocean Eng.,* **124**(4), 157–171.

Titov, V.V., Rabinovich, A.B., Mofjeld, M.O., Thomson, R.E. & González, F.I., 2005. The global reach of the 26 December 2004 Sumatra Tsunami, *Science,* **309**(5743), 2045–2048.

Uslu, B., Borrero, J.C., Dengler, L.A. & Synolakis, C.E., 2007. Tsunami inundation at Crescent City, California generated by earthquakes along the Cascadia Subduction Zone, *Geophys. Res. Lett.,* **34,** L20601, doi:10.1029/2007GL030188.

Wei, Y. *et al*., 2008. Real-time experimental forecast of the Peruvian tsunami of August 2007 for U.S. coastlines, *Geophys. Res. Lett.,* **35,** L04609, doi:10.1029/2007GL032250.

Weinstein, S.A. & Okal, E.A., 2005. The mantle wave magnitude M_m and the slowness parameter Θ: five years of real-time use in the context of tsunami warning, *Bull. Seismol. Soc. Am.,* **95,** 779–799.

Weinstein, S.A., & Lundgren P.R., 2008. Finite fault modeling in a tsunami warning center context, *Pure appl. Geophys.*, **165,** 451–474.

Wichmann, A., 1918. Die Erdbeben des Indischen Archipels bis zum Jahre 1857, *Verhandelingen K. Akad. Wetensch. te Amsterdam, Tweede Sectie,* **20**(4), 193.

Zachariasen, J., Sieh, K., Taylor, F.W., Edwards, R.L. & Hantoro, W.S., 1999. Submergence and uplift associated with the giant 1833 Sumatran subduction earthquake atoll: Evidence from coral microatolls, *J. geophys. Res.,* **104,** 895–919.